Phase Diagrams for Ceramists
Volume IV

Robert S. Roth,

Taki Negas, and

Lawrence P. Cook

Compiled at the National Bureau of Standards

Geraldine Smith, *Editor*

The American Ceramic Society

65 Ceramic Drive, Columbus, Ohio 43214

Printed in U.S.A.

Ce-Zr-O

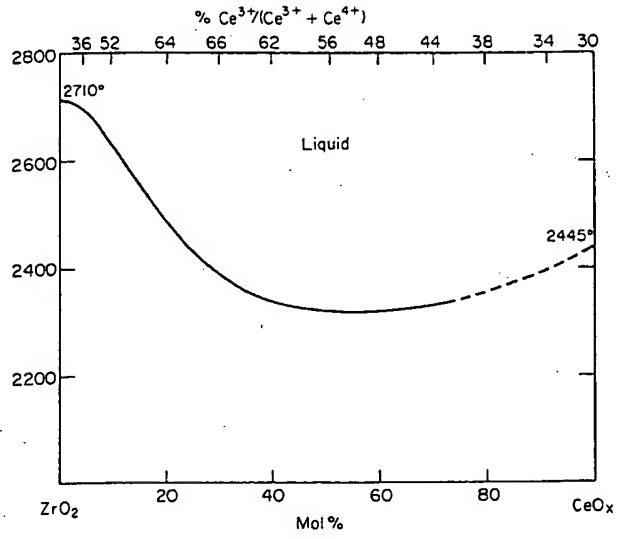

FIG. 5042.—System ZrO_2–CeO_x.
A. Rouanet, *C. R. Hebd. Seances Acad. Sci., Ser. C.*, **266** [12] 908 (1968).

Ten compositions were formulated from ZrO_2 and CeO_2 of unspecified starting purity. Specific experimental details related to pretreatment of samples are not given but generalized methods can be found in Ref. 1. The liquidus curve was established using a solar furnace and thermal analysis methods in air.[1,2] Fused samples were quenched in water or in air, examined by powder X-ray diffraction, and reoxidized at 800° in air. Associated weight gains were used to calculate the degree of reduction of quenched liquids.

Figure 355 shows generalized subsolidus relations for the system ZrO_2–CeO_2 (in air) excluding the tetragonal ↔ cubic transition for ZrO_2-rich compositions. Reduction of the cerium oxide component at subsolidus and liquidus temperatures also is not suggested. This diagram provides a more reliable liquidus with a minimum suggested near 60 mol% cerium oxide and ≈2310°. The approximate Ce^{3+} content at the liquidus temperature [$Ce^{3+}/(Ce^{3+} + Ce^{4+})$(%)] (shown on top of diagram) was recalculated from graphical data presented. Note that reduction is extensive from cerium oxide ($CeO_{\approx 1.85}$, 2445°) to a maximum near 70 mol% ZrO_2. Liquidus temperatures for compositions having <25 mol% ZrO_2 are subjected to greater error because of the vaporization of the cerium oxide component. X-ray data for quenched but recrystallized liquids and for reoxidized materials are given.

1. A. Rouanet, Thesis, University of Montpellier, 1970; 109 pp.
2. M. Foex, *Rev. Int. Hautes Temp. Refract.*, 3 [3] 309 (1966).
T.N.

Co-Li-O

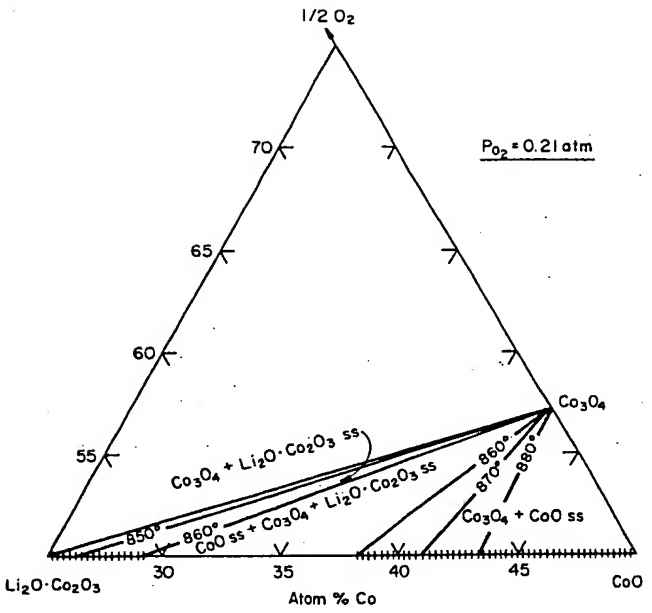

FIG. 5043.—System Li–Co–O.
R. J. Moore and J. White, *J. Mater. Sci.*, 9 [9] 1401 (1974).

The starting materials appear to have been of ordinary reagent grade purity, although precise details are not supplied. Equilibrium relationships were established in air using a thermobalance. Prefired pellets were prepared by heating Li_2CO_3-Co_3O_4 mixtures in air at 800° for 3 h. The compositions of the pellets were determined by quantitative flame-photometric analysis for Li. The pellets were first equilibrated on the thermobalance at 930° and brought into equilibrium at progressively lower temperatures. Although much Li loss occurred during the initial firing, Li loss was negligible during the actual equilibrations on the thermobalance. Five compositions were studied at closely spaced temperatures between 800° and ≈950°; an isobaric phase diagram was constructed from the weight changes. Up to 860°, mixtures in equilibrium with air consisted of a two-phase assemblage (Co_3O_4 and $LiCoO_2$ ss) but, at 860°, they enter the three-phase triangle ($LiCoO_2$ ss + Co_3O_4 + CoO ss) while above this temperature the stable assemblage is (CoO ss + Co_3O_4). This interpretation was confirmed by microscopic examination of polished sections. The diagram shows the position of the two-phase tie lines at 850°, 870°, and 880° as well as the three-phase assemblage at 860°. Limits of solid solution on the $Li_2O \cdot Co_2O_3$–CoO join are shown by cross-hatching.
F.P.G.

Dy_2O_3–ZrO_2

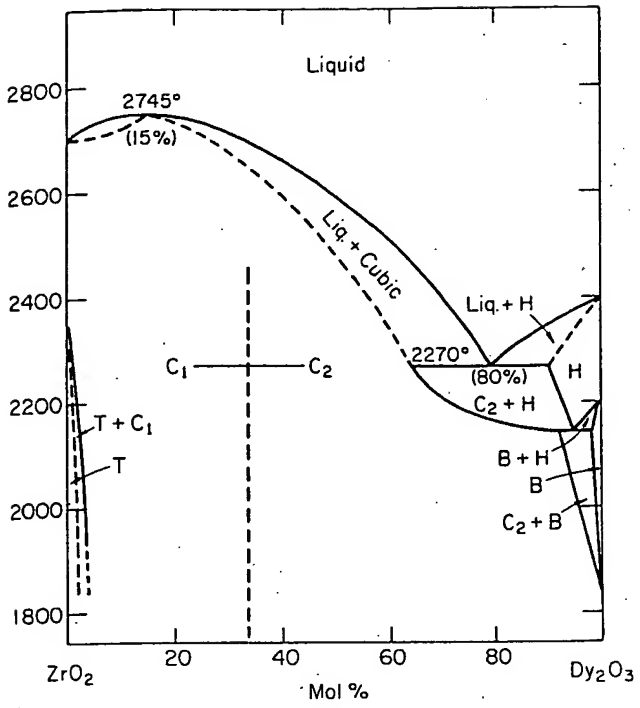

FIG. 5211.—System ZrO_2–Dy_2O_3. B = monoclinic phase, C_1 = cubic ss of the CaF_2 type, C_2 = cubic ss of the Tl_2O_3 type, H = hexagonal ss, T = tetragonal ss having narrow limits of existence near compounds.

A. Rouanet, *Rev. Int. Hautes Temp. Refract.*, 8 [2] 161 (1971).

Liquidus curves and phase transformations in the solid state were obtained with the methods described in Fig. 5232. All dashed curves are estimated. ZrO_2 (99.9% without HfO_2) and Dy_2O_3 (99.9%) were the starting materials. For the polymorphism of ZrO_2 and Dy_2O_3 see Fig. 4259 and Ref. 1, respectively. In the zirconia-rich side, the T → C_1 transition is reversible. Above 2000°, solid solutions vary from a cubic fluorite structure (C_1, ZrO_2-rich side) to a cubic Tl_2O_3-type structure (C_2, Dy_2O_3-rich side). The author states that the C_1 → C_2 transition is continuous with a theoretical boundary at the $2ZrO_2$:Dy_2O_3 composition. The ordered compound of the M_7O_{11} type, reported by Perez y Jorba,[2] was not found. On the Dy_2O_3-rich side, the H phase shows a eutectoid decomposition at 2150° giving C_2 + B (composition of the eutectoid, 5%ZrO_2-95%Dy_2O_3). To better define this system (especially the C_1 → C_2 transition), additional studies involving long term equilibration in the 1800° to 2200° range appear necessary.

1. M. Foex, *Rev. Int. Hautes Temp. Refract.*, 3 [3] 309 (1966).
2. M. Perez y Jorba, *Ann. Chim. (Paris)*, 7 [7-8] 479 (1962).

J.P.C.

Dy_2O_3–MoO_3

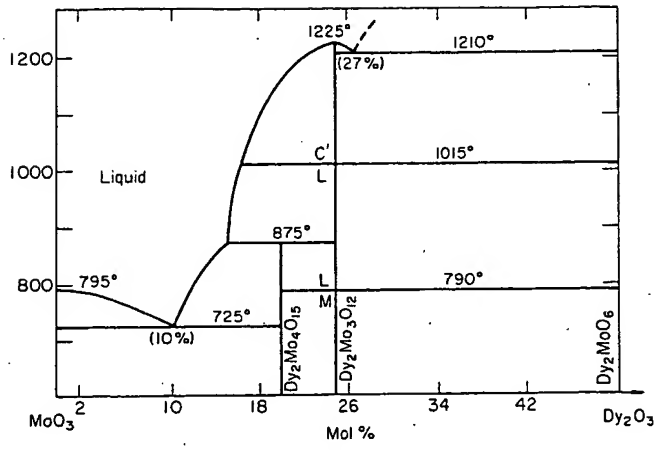

FIG. 5212.—System MoO_3–Dy_2O_3.

G. V. Lysanova, L. Z. Gokhman, and N. G. Evdokimova, *Izv. Akad. Nauk SSSR, Neorg. Mater.*, 7 [11] 2025 (1971); *Inorg. Mater. (Engl. Transl.)*, 7 [11] 1802 (1971).

Mixtures of the oxides were subjected to stagewise annealing with intermediate grindings. The initial annealing temperature was not more than 500° to avoid loss of MoO_3 by volatilization; the temperature was then raised gradually by 100° after every 10 to 20 h. The final annealing temperature for samples with 2 to 18 mol% Dy_2O_3 was 630°; for 20 to 24 mol% Dy_2O_3, 700°; for 25 to 60 mol% Dy_2O_3, 1000° to 1100°; for 60 to 100 mol% Dy_2O_3, 1200°. The duration of annealing at the final temperature was 150 to 250 h. Samples after annealing were analyzed for MoO_3 content, but results are not given. Phase relations in the system were determined by DTA, X-ray diffractometry, and densimetric analysis.

$Dy_2Mo_3O_{12}$ exists in three forms (M, L, and C'). Rapid cooling to room temperature was required for the preparation of C' from either the mixture of starting oxides or M- and L-forms. Slow cooling produced the L-form (the L to M transition is extremely sluggish). The C'-form is hygroscopic. Unindexed X-ray diffraction data are given.

L.L.Y.C.

Dy_2O_3–WO_3

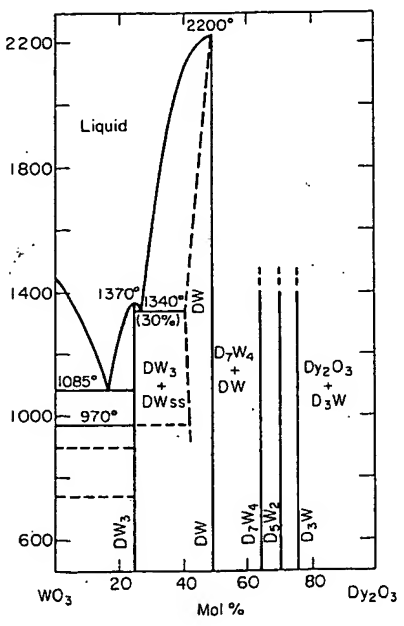

Er_2O_3–TiO_2 (concl.)

FIG. 5216.—System TiO_2–Er_2O_3. R = rutile (TiO_2); P = pyrochlore-type $Er_2Ti_2O_7$ ss; F = fluorite-type $Er_2Ti_2O_7$ ss; C = cubic Er_2O_3.

I. Leban, D. Kolar, and Lj. Golic, *Monatsh. Chem.*, 103 [4] 1044 (1972).

Laboratory pure Er_2O_3 and TiO_2 were blended, prefired to 1300°, reground, and finally heated on Pt sheets for 5 to 10 h at 1500°, 1550°, and 1600° followed by rapid cooling. Phases were identified microscopically and with X-ray diffraction.

The pyrochlore compound, $Er_2Ti_2O_7$, exists as a solid solution from 33.3 mol% Er_2O_3 to ≈50 mol% Er_2O_3 where it transforms into a fluorite-type (disordered) solid solution. The upper limit of the fluorite solution is ≈57 mol% Er_2O_3 at 1550° and shifts slightly with temperature. X-ray data are given for various compositions of the pyrochlore and fluorite phases.

Below 1600°, virtually no TiO_2 is soluble in the C-type Er_2O_3 phase. M.F.B.

Er_2O_3–ZrO_2

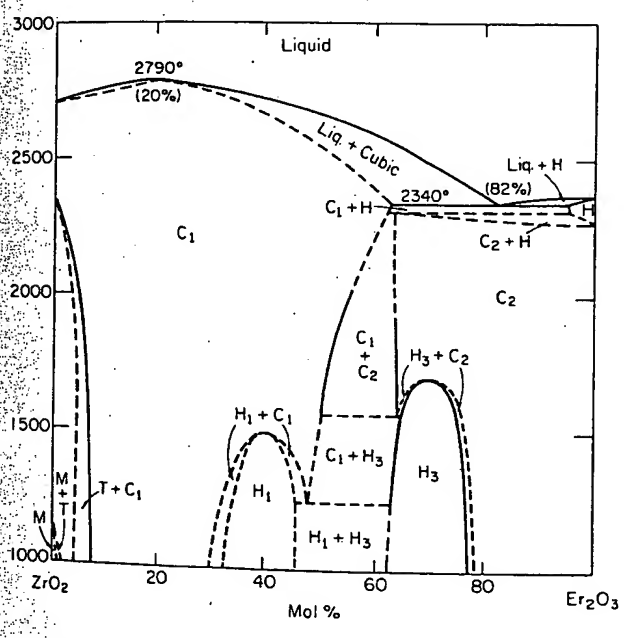

FIG. 5217.—System ZrO_2–Er_2O_3. C_1 = cubic ss of the CaF_2 type, C_2 = cubic ss of the Tl_2O_3 type, H = hexagonal ss, H_1 = hexagonal compound M_7O_{12}, H_3 = hexagonal compound of type M_7O_{11}, M = monoclinic ss, T = tetragonal ss.

A. Rouanet, *Rev. Int. Hautes Temp. Refract.*, 8 [2] 161 (1971); P. Duran, *J. Am. Ceram. Soc.*, 60 [11-12] 510 (1977).

Liquidus curves and phase transformations in the solid state were obtained with the methods described in Fig. 5231. All dashed curves are estimated. Starting materials for both studies were ZrO_2 (99.9% without HfO_2) and Er_2O_3 (99.9%). See Fig. 4259 and Ref. 1 for the polymorphism of ZrO_2 and Er_2O_3, respectively.

For the zirconia-rich side, a detailed study of the monoclinic (M), tetragonal (T), and cubic (C_1) relations is given by Duran. The melting point of Er_2O_3 is taken from Ref. 2. At high temperature (>2000°), solid solutions vary from a cubic fluorite structure (C_1) to a cubic Tl_2O_3-type structure (C_2). Rouanet states that the $C_1 \rightarrow C_2$ transition is continuous with a theoretical boundary at the $2ZrO_2$:Er_2O_3 composition. By long time annealing and quenching, Duran found new phases in the 1000° to 2000° range. In the 25% to 45% Er_2O_3 range, an ordered, hexagonal phase of the M_7O_{12} type ($Zr_3Er_4O_{12}$) is stable. Near 1500°, it decomposes to C_1 solid solution. In the 60% to 80% Er_2O_3 range another hexagonal compound of the M_7O_{11} type was found but it decomposes above 1700°. This ordered compound is similar to Er_6HfO_{11}, previously found by Spiridonov and Komissarova,[3] and to the hexagonal phase (H_3) reported by Perez y Jorba[4] for the ZrO_2-Gd_2O_3, ZrO_2-Dy_2O_3, and ZrO_2-Yb_2O_3 systems. Between the two monophasic regions, biphasic areas are present, particularly the $C_1 + C_2$ region between 1500° and 2000° within the 50% to 60% Er_2O_3 range. This diagram remains tentative but demonstrates clearly that additional studies above 2000° are necessary to better characterize the system.

1. M. Foex and J. P. Traverse, *Rev. Int. Hautes Temp. Refract.*, 3 [3] 309 (1966).
2. J. P. Coutures, R. Verges, and M. Foex, *ibid.*, 12 [2] 181 (1975).
3. F. M. Spiridonov and L. N. Komissarova, *Zh. Neorg. Khim.*, 15 [3] 875 (1970); *Russ. J. Inorg. Chem. (Engl. Transl.)*, 15 [3] 445 (1970).
4. M. Perez y Jorba, *Ann. Chim. (Paris)*, 7 [7-8] 479 (1962).

J.P.C.

Er_2O_3–MoO_3

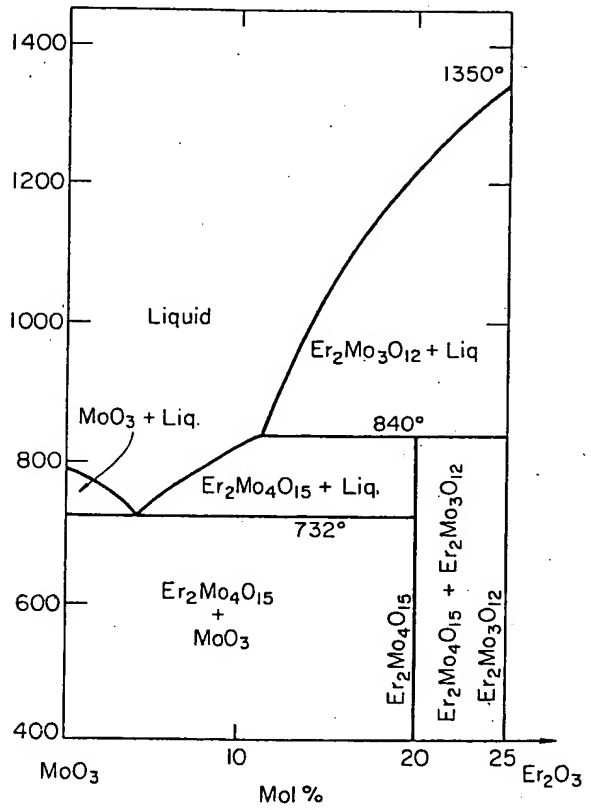

FIG. 5218.—System MoO_3–Er_2O_3.

S. S. Antonova, I. V. Shakno, and V. E. Plyushchev, *Izv. Vyssh. Uchebn. Zaved., Khim. Khim. Tekhnol.*, 14 [1] 17 (1971).

Samples were prepared by prolonged heating and slow cooling of oxide mixtures in air at 500° to 650°. Analysis was carried out by DTA and X-ray diffractometry. Unit cell parameters of the incongruently melting compound $Er_2Mo_4O_{15}$ (1:4) are given. The system is qualitatively similar to the systems MoO_3–Y_2O_3 and MoO_3–Sm_2O_3, described in the same reference (Figs. 5254 and 5246). D.K.

Gd_2O_3–ThO_2

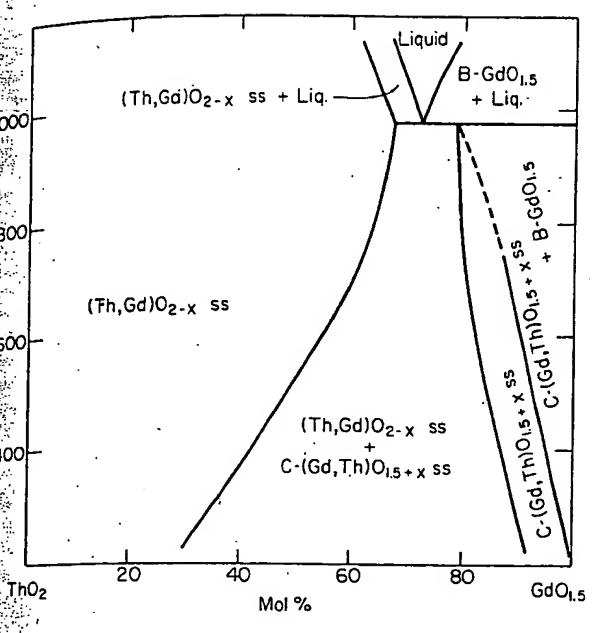

FIG. 5222.—System ThO_2–$GdO_{1.5}$.
C. Keller, U. Berndt, H. Engerer, and L. Leitner, *J. Solid State Chem.*, 4 [3] 453 (1972).

Coprecipitation of hydroxides was compared to direct mixing. Evaluation of the approach to equilibrium indicated coprecipitation to be superior and this method was used in sample preparation. High temperature X-ray phase analysis and room temperature quenches were compared, and the results indicated that room temperature quenches were accurately representative of the high temperature patterns. Thus, quenched samples were used for phase determinations. The temperature range considered was 1250° to 2100°. Based on density measurements, the anion vacancy model is verified for thoria–lanthanon systems.

The coincidence (in temperature) of eutectic (?) melting with $(Gd,Th)O_{1.5+x}$ ss decomposition is not allowed by the phase rule; perhaps peritectic and eutectic melting occur at closely spaced intervals. See also Figs. 4415 and 5223. D.R.W.

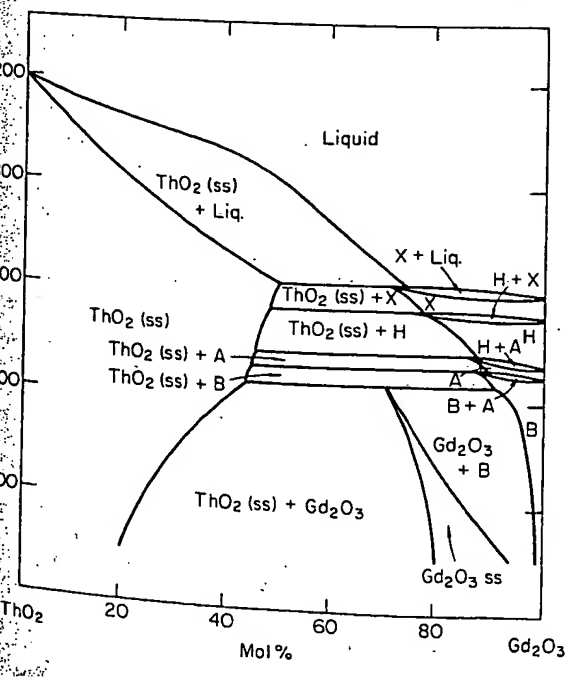

FIG. 5223.—System ThO_2–Gd_2O_3. B = monoclinic (ss), A, H = hexagonal (ss), X = cubic (ss).
F. Sibieude and M. Foex, *J. Nucl. Mater.*, 56 [2] 229 (1975).

The liquidus curve and phase transformations in the solid state were obtained by methods described in Fig. 5231. The liquidus and solidus curves between ThO_2 and 50%ThO_2-50%Gd_2O_3 are estimated.

This diagram is tentative and based on experimental results obtained by thermal analysis and high temperature X-ray diffraction and data for the polymorphism of Gd_2O_3.[1]

The liquidus curve is characterized by a peritectic found on the Gd_2O_3-rich side (≈18%ThO_2-82%Gd_2O_3) at 2400°.

In contrast to the ThO_2–La_2O_3, ThO_2–Nd_2O_3, and ThO_2–Sm_2O_3 systems, no ordered phases were found, and the solution of Gd_2O_3 in cubic ThO_2 increases rapidly with temperature. The C, B, A, H, and X phases of Gd_2O_3 show peritectoid decomposition. This diagram is in good agreement with Fig. 4415.

1. M. Foex and J. P. Traverse, *Rev. Int. Hautes Temp. Refract.*, 3 [4] 429 (1966). J.P.C.

Gd_2O_3–ZrO_2

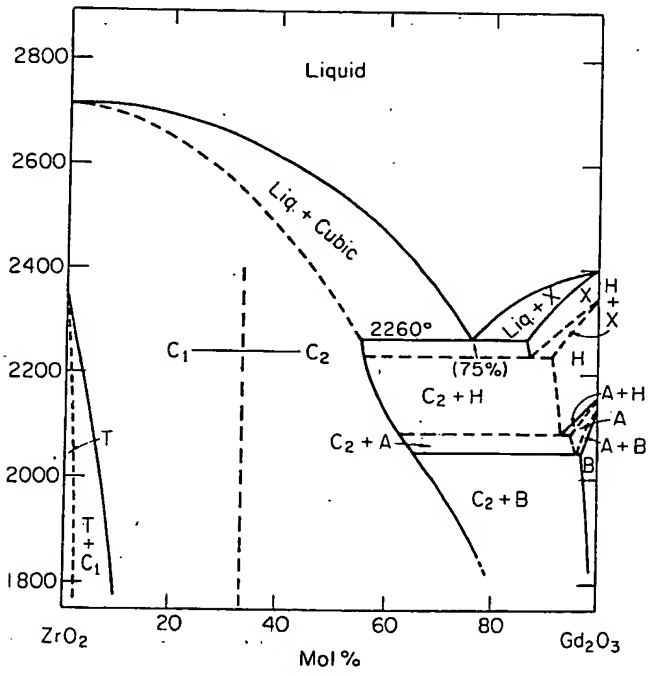

FIG. 5224.—System ZrO_2–Gd_2O_3.
A. Rouanet, *Rev. Int. Hautes Temp. Refract.*, 8 [2] 161 (1971).

Liquidus curves and phase transitions in the solid state were obtained by methods described in Fig. 5232. All dashed curves are estimated. ZrO_2 (99.9% without HfO_2) and Gd_2O_3 (99.9%) were the starting materials. See Fig. 4259 and Ref. 1 for the polymorphism of ZrO_2 and Gd_2O_3, respectively.

For the Gd_2O_3-rich portion, this work differs significantly from Fig. 2369, which was constructed using coprecipitated materials, followed by annealing at various temperatures, in some cases over 2000°. One of the major differences is the stability of a hexagonal (H), ordered phase. The X phase could not be quenched and was difficult to study at high temperature (to near the melting point) due to preferential vaporization of Gd_2O_3. Therefore, its homogeneity range could not be determined. The original diagram shows a

Gd_2O_3–ZrO_2 (concl.)

peritectic point near 10%ZrO_2–90%Gd_2O_3 but this is questionable based on data in Ref. 1. This region is redrawn to include a limited stability range for a biphasic region, C_2 + X. The hexagonal (H) form in the original diagram has a eutectoid decomposition at 2050° (10%ZrO_2–90%Gd_2O_3) giving C_2 + B. However, because of the Gd_2O_3 polymorphism, the moderate temperature range of the Gd_2O_3-rich side also is redrawn (see commentary for Fig. 5245).

On the zirconium-rich side, this diagram differs from Fig. 2370. As shown in Fig. 2369, however, an ordered pyrochlore compound ($Gd_2Zr_2O_7$) is stable but disorders above ≈1550° which is below the temperature range of this study. The tetragonal (T) → C_1 transition is reversible. The author states that the C_1 → C_2 (cubic fluorite → cubic Tl_2O_3) transition appears to be continuous with a theoretical boundary at the pyrochlore composition.

This diagram appears to be the best available. However the C_1 → C_2 transition (a biphasic region must exist) and the Gd_2O_3-rich side could be better defined.

1. M. Foex and J. P. Traverse, *Rev. Int. Hautes Temp. Refract.*, 3 [4] 429 (1966). J.P.C.

Gd_2O_3–MoO_3

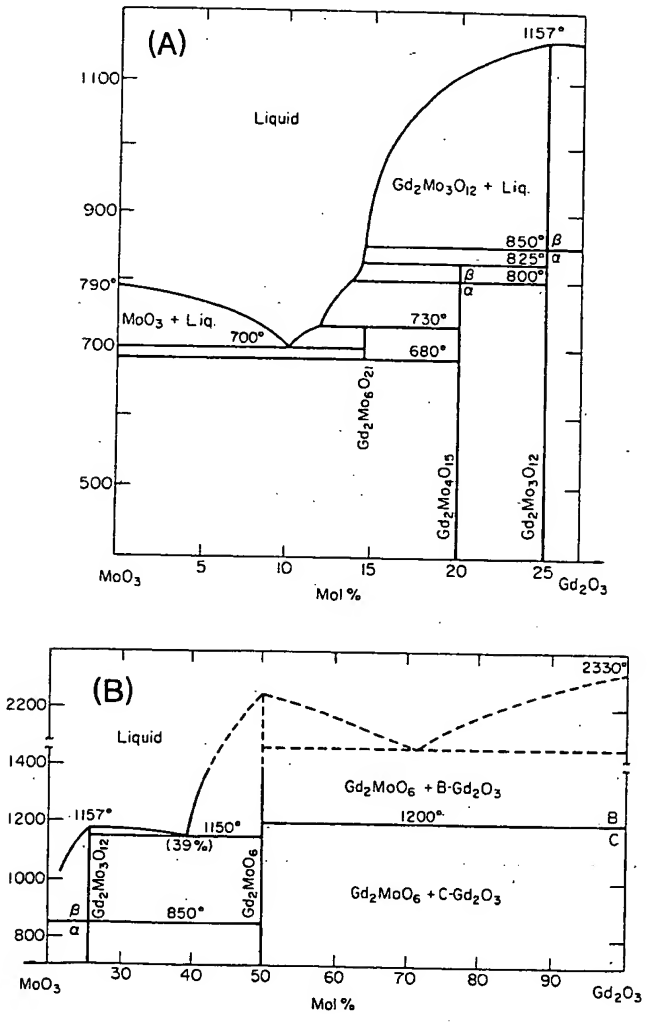

FIG. 5225.—System MoO_3–Gd_2O_3. (*A*) MoO_3-rich portion and (*B*) region between 25 and 100 mol% Gd_2O_3.

K. Megumi, H. Yumoto, S. Ashida, S. Akiyama, and Y. Furuhata, *Mater. Res. Bull.*, 9 [4] 391 (1974).

Gd_2O_3 and MoO_3 of specpure grade were used as starting materials. They were mixed for 5 h in dried air, pelletized, and sintered to prepare the samples. DTA and X-ray diffractometry were used for the determination of phase relations. Samples exhibiting multiple heat anomalies were measured more than twice by changing cycling rate and the quantity of the samples to reproduce the DTA curves.

In (*A*), two compounds were found. The composition of the MoO_3-rich compound, although given as $Gd_2Mo_6O_{21}$, is not well established based on experimental data presented. Two DTA maximums were observed for $Gd_2Mo_4O_{15}$ at 825° and 800°, illustrating a peritectic reaction and a phase transition, respectively. The phase transition was not confirmed by X-ray diffractometry.

In (*B*), only $Gd_2Mo_3O_{12}$ and Gd_2MoO_6 were found to be stable phases. Attempts made to synthesize both $Gd_{18}Mo_4O_{39}$ and Gd_6MoO_{12}[1] failed. $Gd_2Mo_3O_{12}$ is dimorphic with a transition temperature detected at 850°. The transition from α (low temperature) form to β (high temperature) form is instantaneous, whereas the reverse reaction is very sluggish. The reported γ form[2] was not found. Unindexed X-ray powder diffraction data are given.

1. F. P. Alekseev, E. I. Get'man, G. G. Koshcheev, and M. V. Mokhosoev, *Zh. Neorg. Khim.*, **14** [11] 2954 (1969); *Russ. J. Inorg. Chem. (Engl. Transl.)*, **14** [11] 1558 (1969).
2. K. Nassau, P. B. Jamieson, and J. W. Shiever, *J. Phys. Chem. Solids*, **30** [5] 1225 (1969). L.L.Y.C.

Ho_2O_3–ThO_2

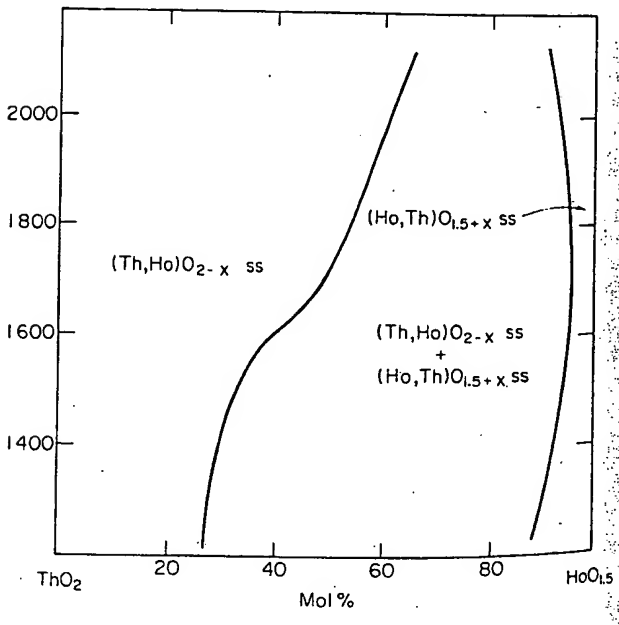

FIG. 5226.—System ThO_2–$HoO_{1.5}$.

C. Keller, U. Berndt, H. Engerer, and L. Leitner, *J. Solid State Chem.*, **4** [3] 453 (1972).

Coprecipitation of hydroxides was compared to direct mixing. Evaluation of the approach to equilibrium indicated that coprecipitation was superior and this method was used in sample preparation. High temperature X-ray phase analysis and room temperature quenches were compared and the results indicated that room temperature quenches were accurately representative of the high temperature patterns. Thus, quenched samples were used for phase determinations. The temperature range considered was 1250° to 2100°. Based on density measurements, the anion vacancy model is verified for thoria-lanthanon systems. Compare with Fig. 5227. D.R.W.

Ho_2O_3–ThO_2 (concl.)

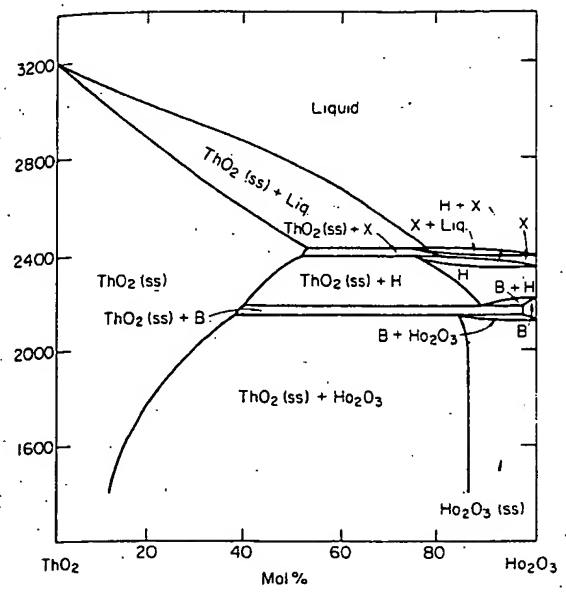

FIG. 5227.—System ThO_2–Ho_2O_3. B = monoclinic (ss), H = hexagonal (ss), X = cubic (ss).
F. Sibieude and M. Foex, *J. Nucl. Mater.*, 56 [2] 229 (1975).

The liquidus curve and phase transformations in the solid state were obtained by methods described in Fig. 5231. The liquidus and solidus curves between ThO_2 and 45%ThO_2-55%Ho_2O_3 are estimated.

This diagram is tentative and is based on experimental results obtained by thermal analysis and high temperature X-ray diffraction and data for the polymorphism of Ho_2O_3.[1] This diagram, except for the stability range of the B, H, and X forms of Ho_2O_3, is identical to that for the system ThO_2–Dy_2O_3.

1. M. Foex and J. P. Traverse, *Rev. Int. Hautes Temp. Refract.*, 3 [4] 429 (1966). J.P.C.

Ho_2O_3–ZrO_2

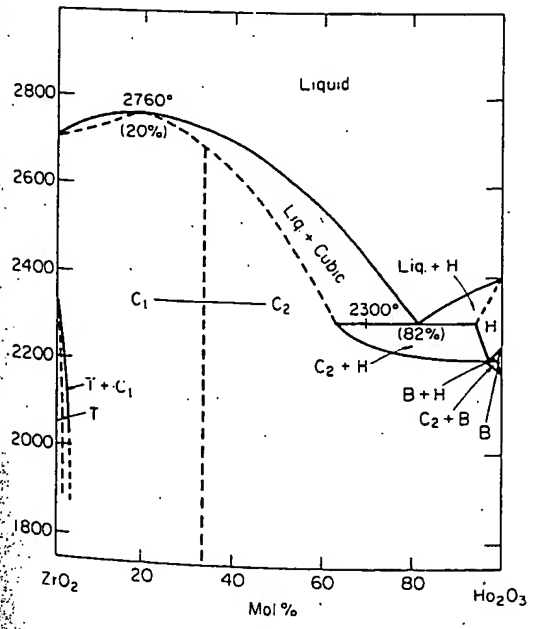

FIG. 5228.—System ZrO_2–Ho_2O_3. B = monoclinic structure, C_1 = cubic ss of CaF_2 type, C_2 = cubic ss of Tl_2O_3 type, H = hexagonal ss, T = tetragonal ss.
A. Rouanet, *Rev. Int. Hautes Temp. Refract.*, 8 [2] 161 (1971).

Liquidus curves and phase transformations in the solid state were obtained by methods described in Fig. 5232. All dashed curves are estimated. ZrO_2 (99.9% without HfO_2) and Ho_2O_3 (99.9%) were the starting materials. For the polymorphism of ZrO_2 and Ho_2O_3, see Fig. 4259 and Ref. 1, respectively. This diagram is similar to Fig. 5211 and similar comments are pertinent.

1. M. Foex and J. P. Traverse, *Rev. Int. Hautes Temp. Refract.*, 3 [4] 429 (1966). J.P.C.

La_2O_3–GeO_2

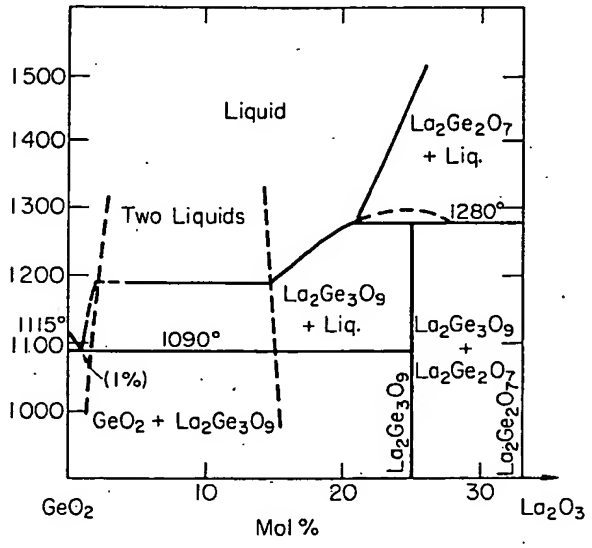

FIG. 5229.—System GeO_2–La_2O_3.
N. G. Gutkina, I. I. Kozhina, and L. K. Shmatock, *Izv. Akad. Nauk SSSR, Neorg. Mater.*, 7 [8] 1382 (1971); *Inorg. Mater. (Engl. Transl.)*, 7 [8] 1228 (1971).

Synthesis was carried out in Pt crucibles using cp grade GeO_2 and La_2O_3 with heating to 1500°–1640°. Analysis was accomplished by application of polythermal, optical, X-ray diffraction, and ir methods to quenched specimens that were annealed isothermally and in temperature gradients.

The diagram indicates the temperature at which flow of crystallized fragments occurred on heating and probably does not represent the true liquidus. It is said to be an approximate equilibrium diagram. A region of immiscibility was found in melts at high GeO_2 contents. $La_2Ge_2O_7$ melts congruently and forms a metastable eutectic with the incongruently melting $La_2Ge_3O_9$. The latter phase forms a true eutectic with GeO_2 at 1090° and 1 mol% La_2O_3. Refractive index values of vitreous and crystalline phases are listed in a table. M.F.B.

La_2O_3-ZrO_2

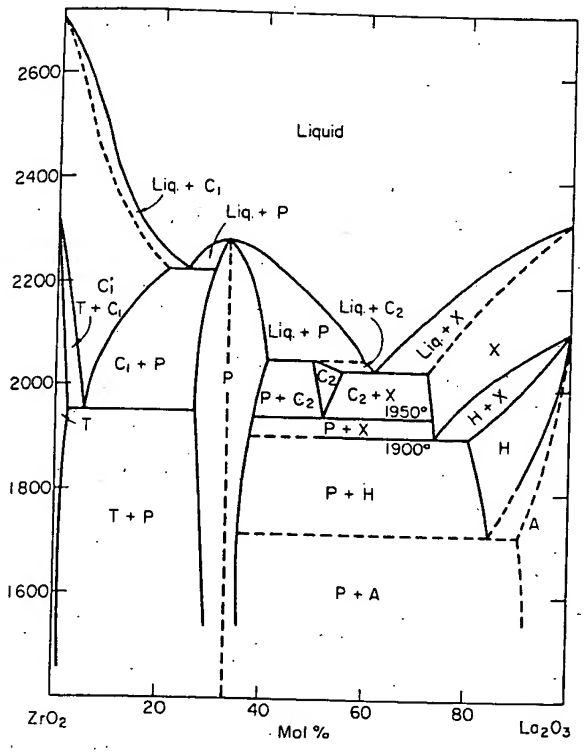

FIG. 5232.—System ZrO_2–La_2O_3. A = hexagonal ss, C_1 = cubic ss of the CaF_2 type, C_2 = cubic ss of the Tl_2O_3 type, H = hexagonal ss, P = pyrochlore-type compound, T = tetragonal ss, X = cubic ss.
A. Rouanet, *Rev. Int. Hautes Temp. Refract.*, 8 [2] 161 (1971).

The liquidus curve was obtained from cooling curves obtained with a thermal analysis device associated with a 2 kW horizontal axis solar furnace.[1] Solidus curves (dashed lines) were estimated. To prevent contamination, runs were performed in air without crucibles. Temperatures were measured by optical pyrometry assuming an average emissivity of 0.5. The pyrometer (0.65 μm with a Cs cell) was calibrated against the melting points of ZrO_2 (2710°) and Al_2O_3 (2050°). Phase transitions above 1800° were observed by high temperature X-ray diffraction using a Re ribbon under reducing conditions (He + ≈10% H_2). These conditions could affect temperature measurements associated with phase transitions. Samples were premelted in air using solar furnaces, finely crushed, and deposited on the heating element.

The purity of the ZrO_2 starting material was 99.9% (excluding HfO_2) and that of the La_2O_3 was 99.99%. The diagram shows a definite compound (pyrochlore phase type) with a congruent melting point (2280°) surrounded by two eutectics, 75%ZrO_2-25%La_2O_3 (2220°) and 37.5%ZrO_2-62.5%La_2O_3 (2030°). Cabannes *et al.*[2] measured the melting point of the first eutectic in air and in oxygen (2224° ±10°). In argon, the reduction of ZrO_2 decreases the melting point by 45°. For polymorphism of ZrO_2 see Fig. 4259, and for La_2O_3, see Ref. 3.

The apparent inflection on the liquidus curve between ZrO_2 and the ZrO_2-$La_2Zr_2O_7$ eutectic remains unexplained but corresponds to the experimental data.

The X phase could not be quenched and was difficult to study at high temperature because of excessive vaporization of La_2O_3 near 2100°. Consequently, its homogeneity range could not be determined accurately. At 1900°, the maximum solubility of ZrO_2 is ≈30%. The X → H transition was observed easily by thermal analysis up to 15% of ZrO_2. The H → A transformation, observed sharply for pure La_2O_3, is not well defined for solid solutions. Nevertheless, the phase transition temperature decreases sharply as the ZrO_2 concentration increases. The eutectoid reaction at 1900° was determined by high temperature X-ray diffraction.

Although the C_2 phase (C_2: cubic-type Tl_2O_3) doesn't exist at high temperature for La_2O_3, solution of ZrO_2 can stabilize this structure. The stability range (*T* and composition) is very limited but observed by high temperature X-ray diffraction. This C_2 phase shows a eutectoid transformation (eutectoid point 48%ZrO_2-52%La_2O_3, 1950°) giving P and X phases.

The cubic $La_2Zr_2O_7$ compound is stable to the melting point. Thermal expansion was measured by high temperature X-ray diffraction.

On the zirconia-rich side, the C_1 cubic phase shows a eutectoid transformation (eutectoid point 93%ZrO_2-7%La_2O_3, 1950°) giving T and P phases. The T — C_1 transition is reversible.

This diagram differs from previous, incomplete diagrams (Figs. 346, 2374, 2375). It should be considered the best available. Future work is necessary to determine the precise stability range of the C_2 solid solution and to provide an explanation of the inflection on the liquidus curve between ZrO_2 and the ZrO_2-$La_2Zr_2O_7$ eutectic.

1. M. Foex, *Rev. Int. Hautes Temp. Refract.*, 3 [3] 309 (1966).
2. F. Cabannes, J. Simonato, M. Foex, and J. P. Coutures, *High Temp.-High Pressures*, 4 [5] 589 (1972).
3. M. Foex and J. P. Traverse, *Rev. Int. Hautes Temp. Refract.*, 3 [4] 429 (1966).

J.P.C.

Lu_2O_3-ThO_2

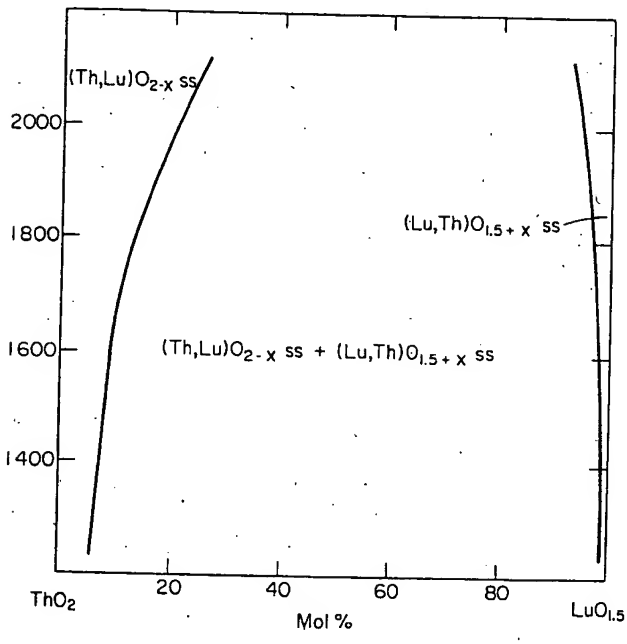

FIG. 5233.—System ThO_2–$LuO_{1.5}$.
C. Keller, U. Berndt, H. Engerer, and L. Leitner, *J. Solid State Chem.*, 4 [3] 453 (1972).

Coprecipitation of hydroxides was compared to direct mixing. Evaluation of the approach to equilibrium indicated that coprecipitation was superior and this method was used in sample preparation. High temperature X-ray phase analysis and room temperature quenches were accurately representative of the high temperature patterns. Thus, quenched samples were used for phase determinations. The temperature range considered was 1250° to 2100°. Based on density measurements, the anion vacancy model is verified for thoria–lanthanon systems.

D.R.W.

Nd_2O_3–Yb_2O_3 (concl.)

The cubic C phase of Yb_2O_3 dissolves up to ≈30 mol% Nd_2O_3. Premelted samples which were subsequently annealed at 1400° exhibited at room temperature a linear increase in lattice parameter with Nd_2O_3 addition.

At normal pressures, there are no temperature ranges in which either Nd_2O_3 or Yb_2O_3 are stable in the monoclinic B form. However, when Yb_2O_3 is added to Nd_2O_3 in solid solution at lower temperatures, a B-type structure is formed (see Fig. 348). The compositional range of the B solid solutions is ≈3 to 40 mol% Yb_2O_3. For a discussion of the Nd_2O_3-rich, B structure solid solution, refer to Fig. 5234.

Pure Nd_2O_3 has the hexagonal A structure at low temperatures and dissolves <1 mol% Yb_2O_3 at 1400°. The solubility increases to a maximum of 35 to 40 mol% Yb_2O_3 at 1940°. The A solid solutions transform to the hexagonal H form at higher temperatures. It is difficult to distinguish between the A and H forms by high-temperature X-ray diffraction. However, thermal arrests can be used to locate the apparent transformation temperatures for the A⇌H transformation.

The H polymorph of Nd_2O_3 forms solid solutions extending nearly to Yb_2O_3. The temperature stability range for the H form shifts with composition. The presence of an H form for pure Yb_2O_3 was not confirmed by X-ray diffraction, but a thermal effect (DTA) which may correspond to the C⟷H transformation was observed near the melting point of Yb_2O_3. Tresvyatskii *et al.*[1] also reported this effect. The addition of 1 to 2 mol% Nd_2O_3 to Yb_2O_3 readily forms the Y polymorph near the melting point.

The H form and X form (cubic) have not been retained at room temperature even by very rapid quenching. This may be due to the ready formation of the metastable and quite persistent B phase.

No compound (e.g. $YbNdO_3$) was found. Refer to Fig. 5234 for a comparison with other Nd_2O_3–lanthanide systems.

1. S. G. Tresvyatskii, L. M. Lopato, A. V. Shevchenko, and A. E. Kushchewskii, *Colloq. Int. CNRS*, 1972, No. 205, p. 247.

M.F.B.

Nd_2O_3–SiO_2

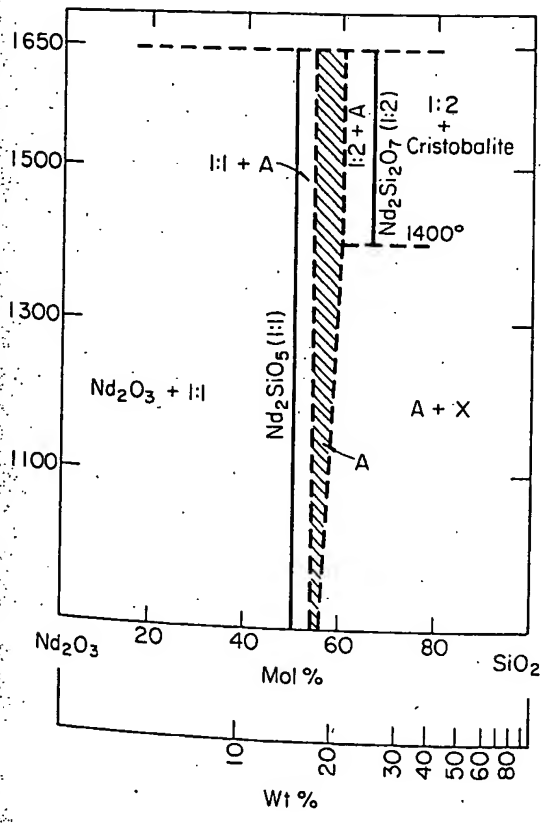

FIG. 5236.—System Nd_2O_3–SiO_2 in air.

N. A. Toporov and M. V. Kougiya, *Izv. Akad. Nauk SSSR, Neorg. Mater.*, 7 [7] 1220 (1971); *Inorg. Mater. (Engl. Transl.)*, 7 [7] 1082 (1971).

Specimens were synthesized by solid state reaction of mixtures of Nd_2O_3 and SiO_2 in air at 1450° to 1650°. Optical, chemical, and X-ray diffraction analyses were used to identify phases.

The compound 1:1 ($Nd_2O_3 \cdot SiO_2$) varied little in composition. The 1:2 compound also varies little in composition above 1400°. Below 1400°, the 1:2 compound decomposes into two phases, in agreement with Miller and Rose (Fig. 2380), who, however, show the decomposition at ≈1540°. The region marked A in the diagram represents one of these phases and corresponds to a composition of 7:9 below 1400° and to a composition of 2:3 (6:9)[1] above that temperature. There is a small solubility of Nd_2O_3 in the A phase which has the apatite structure over the enire temperature range. The second phase, into which the 1:2 compound decomposes below 1400°, is designated the X phase and is a new phase not reported in Figs. 2380 and 2381. This phase is believed to be 1:3 or 1:4 in composition, but these compounds could not be synthesized by direct reaction of the end-member oxides.[2] A partial diffraction pattern is provided for the X phase, but no structural type is assigned.

1. G. J. McCarthy, W. B. White, and R. Roy, *J. Inorg. Nucl. Chem.*, 29 [1] 253 (1967).
2. A. N. Lazarev, Covalent Spectra and the Structure of Silicates, Nauka, Leningrad (1969).

M.F.B.

Nd_2O_3–ThO_2

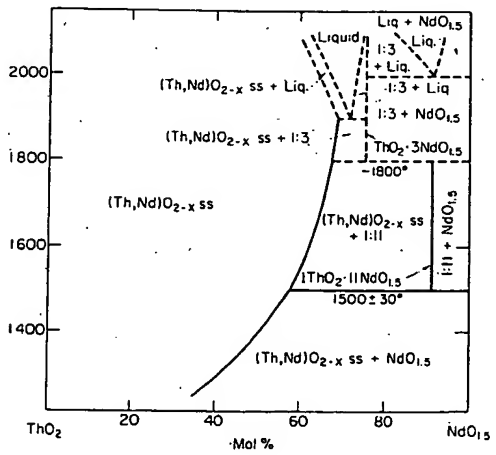

FIG. 5237.—System ThO_2–$NdO_{1.5}$.

C. Keller, U. Berndt, H. Engerer, and L. Leitner, *J. Solid State Chem.*, 4 [3] 453 (1972).

Coprecipitation of hydroxides was compared to direct mixing. Evaluation of the approach to equilibrium indicated that coprecipitation was superior and this method was used in sample preparation. High temperature X-ray phase analysis and room temperature quenches were compared and the results indicated that room temperature quenches were accurately representative of the high temperature patterns. Thus, quenched samples were used for phase determinations. The temperature range considered was 1250° to 2100°. Based on density measurements, the anion vacancy model is verified for thoria–lanthanon systems.

The coincidence (in temperature) of maximum and minimum decomposition of the 1:11 and 1:3 phases is not allowed by the phase rule; perhaps these two reactions occur at closely spaced temperatures. Compare with Fig. 5238.

D.R.W.

Nd_2O_3-ThO_2 (concl.)

Nd_2O_3-ZrO_2

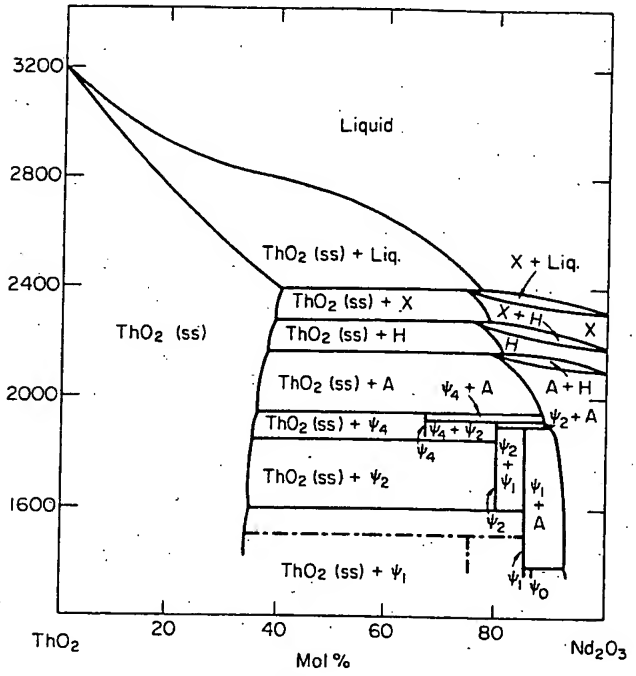

FIG. 5238.—System ThO_2–Nd_2O_3. A, H = hexagonal (ss), X = cubic (ss), ψ_0–ψ_4 = hexagonal compounds.
F. Sibieude and M. Foex, *J. Nucl. Mater.*, **56** [2] 229 (1975).

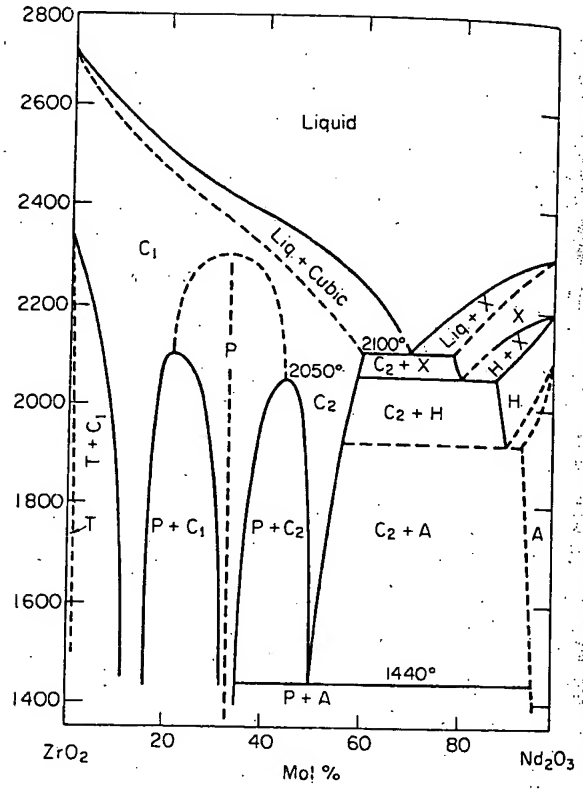

FIG. 5239.—System ZrO_2–Nd_2O_3. A = hexagonal ss, C_1 = cubic ss of the fluorite type, C_2 = cubic ss of the Tl_2O_3 type, H = hexagonal ss, P = pyrochlore-type compound, T = tetragonal ss, X = cubic ss.
A. Rouanet, *Rev. Int. Hautes Temp. Refract.*, **8** [2] 161 (1971).

The liquidus curve and phase transformations in the solid state were obtained by methods described in Fig. 5231. The solidus curve is estimated.

This tentative phase diagram is based on using experimental results obtained by thermal analysis and high temperature X-ray diffraction and the polymorphism of Nd_2O_3.[1]

The liquidus did not show any compound with a congruent melting point, but an inflection near ThO_2 (≈70%ThO_2-30%Nd_2O_3) was found as well as a peritectic point on the Nd_2O_3-rich side (≈25%ThO_2-75%Nd_2O_3) at 2400°. The high volatility of Nd_2O_3 near 2100° made difficult the measurement of the ThO_2 solubility in the H and X forms of Nd_2O_3. Nevertheless, it is obvious that the solubility in Nd_2O_3 increases above 2000° to ≈25% ThO_2 near the fusion point. The A, H, and X phases show a peritectoid decomposition with increasing temperature.

New ordered phases designated Ψ_0, Ψ_1, Ψ_2, Ψ_3, and Ψ_4 were found. Phases Ψ_1 and Ψ_2' were obtained after quenching and were not decomposed by prolonged annealing at 1400°. Phases Ψ_0 and Ψ_3 were also obtained by quenching but decompose after annealing at 1400° giving, respectively, Ψ_1 + A Nd_2O_3, Ψ_2 + ThO_2. The Ψ_4 phase appears between 1850° and 1950°. The composition of the Ψ_0, Ψ_1, Ψ_2, Ψ_3, and Ψ_4 phases is identical to Ψ_0, Ψ_1, Ψ_2, Ψ_3, and Ψ_4 phases observed in the system ThO_2–La_2O_3 (Fig. 5231). The Ψ_3 and Ψ_4 phases appear to be identical in the ThO_2–La_2O_3 and ThO_2–Nd_2O_3 diagrams.[2]

This diagram must be considered the best available for the same reasons mentioned in Fig. 5231, but new studies on the Nd_2O_3-rich side with high resolution electron microscopy would be desirable for a better understanding of the Ψ_0, Ψ_1, Ψ_2, Ψ_3, and Ψ_4 relations.

1. M. Foex and J. P. Traverse, *Rev. Int. Hautes Temp. Refract.*, 3 [4] 429 (1966).
2. F. Sibieude, *J. Solid State Chem.*, 7 [1] 7 (1973). J.P.C.

The liquidus curve was obtained from cooling curves obtained with a thermal analysis device associated with a 2 kW horizontal axis solar furnace.[1] The solidus curves (dashed lines) were estimated. To prevent contamination, runs were performed in air without crucibles. Temperatures were measured by optical pyrometry using an average emissivity of 0.5. The pyrometer was calibrated against the melting points of ZrO_2 (2710°) and Al_2O_3 (2050°). Phase transitions above 1800° were observed by high temperature X-ray diffraction using a Re ribbon under reducing conditions (He + ≈10% H_2). These conditions could alter the temperatures associated with phase transitions. Samples were premelted in air using solar furnaces, finely crushed, and deposited on the heating element.

The purity of ZrO_2 and Nd_2O_3 used as starting materials was 99.9%. In the diagram the apparent inflection on the liquidus curve (at the pyrochlore, P, composition) could be due to a partial ordering of the liquid in this composition range. The melting point and composition of the eutectic between ZrO_2 and Nd_2O_3 are, respectively, 2100° and 30%ZrO_2-70%Nd_2O_3.

The X phase could not be quenched and was difficult to study at high temperature because of the high volatility of Nd_2O_3 near 2100°. Therefore, its stability range could not be determined accurately although the X → H transition temperature decreases with increasing ZrO_2 content. The H → A transformation, easily observed for pure Nd_2O_3, is not clearly defined for solid solutions. At 2060°, the X phase shows a eutectoid decomposition giving C_2 and H (X composition, 20%ZrO_2-80%Nd_2O_3; C_2 composition, 41%ZrO_2-59%Nd_2O_3; H composition, 13%ZrO_2-87%Nd_2O_3). The eutectoid decomposition of C_2 at 1440° yields P and A (C_2 composition, 50%ZrO_2-50%Nd_2O_3; P composition, 65%ZrO_2-35%Nd_2O_3; A composition, 5%ZrO_2-95%Nd_2O_3).

Nd_2O_3–ZrO_2 (concl.)

The compound $Nd_2Zr_2O_7$ does not retain its ordered structure to the melting point. The associated dashed line gives an estimated stability range for the ordered form assuming disorder above 2300° at the $Nd_2Zr_2O_7$ composition. At this composition, the cooling curve[1] shows a thermal arrest at 2250°. This may reflect the order⟷disorder transition. At temperatures lower than 2100°, the solubility of ZrO_2 and Nd_2O_3 in $Nd_2Zr_2O_7$ decreases giving two exsolution fields (P + C_1 and P + C_2).

In the zirconia-rich region the C_1 phase is completely stabilized with an addition of 15 mol% Nd_2O_3. The T → C_1 transition is reversible. This diagram differs in detail from previous, incomplete diagrams (Figs. 350, 2382, 2383) but resembles most closely Fig. 2382. It should be considered the best diagram available. Future work should be performed to better define the immiscibility gaps and the C_1 → P → C_2 transitions.

1. A. Rouanet, Thesis, 1970 reg. CNRS: A.O. 4239. J.P.C.

Pr_2O_3–Y_2O_3

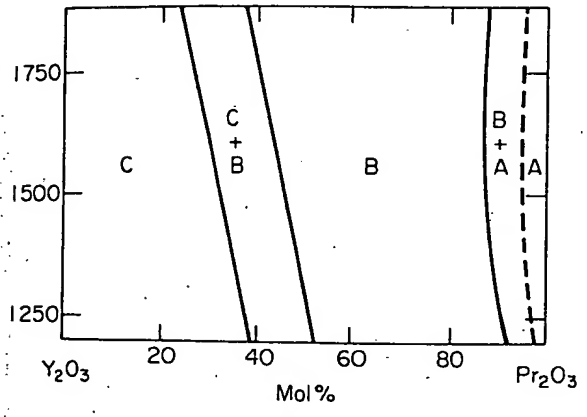

FIG. 5240.—System Y_2O_3–Pr_2O_3. C = cubic phase, B = monoclinic phase, A = hexagonal phase.
P. A. Tikhonov, K. Yu. Merezhinskii, and A. K. Kuznetsov, *Dokl. Akad. Nauk SSSR*, 222 [6] 1387 (1975); *Dokl. Phys. Chem. (Engl. Transl.)*, 222 [6] 650 (1975).

The starting materials consisted of 99.9% Y_2O_3 and 99.8% Pr_6O_{11}. The oxides were mixed, pelletized, and heated at 1750° for 3 h in vacuum (10^{-1} mm Hg). Specimens were then heat-treated at 1250° (10 h), 1500° (5 h), and 1800° (2 h) in a vacuum of 10^{-3} mm Hg, followed by quenching. Phases present were identified by X-ray diffraction.

Broad bands of solid solutions were found corresponding to the standard C and B forms of the rare earth oxide structures.[1] A narrow range of A-type solid solutions was found at high Pr_2O_3 contents. Within the C and B structural types, the unit cell volume increased linearly with increasing mol% Pr_2O_3. The volume of the A unit cell also increased with increasing Pr_2O_3 content, but only two points were determined.

The authors speculate that, while B forms for all rare earth oxides except Y_2O_3 have been found at high pressures,[2,3] linear extrapolation of the B lattice parameters for Y_2O_3-Pr_2O_3 solid solutions to 0% Pr_2O_3 is a valid method for estimating the lattice parameters for the as yet undiscovered B form of Y_2O_3.

1. J. D. McCullough and J. D. Britton, *J. Am. Chem. Soc.*, 74 [20] 5225 (1952).
2. H. R. Hoekstra and K. A. Gingerich, *Science*, 146 [3648] 1163 (1964).
3. H. R. Hoekstra, *Inorg. Chem.*, 5 [5] 754 (1966). M.F.B.

R_2O_3–ZrO_2

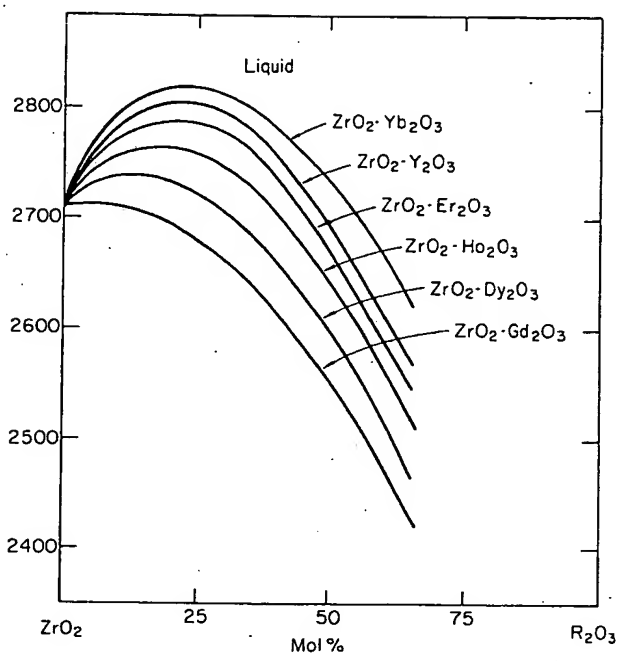

FIG. 5241.—System ZrO_2–R_2O_3 (rare earth oxides).
F. Sibieude and A. Rouanet, *Colloq. Int. CNRS*, 1972, No. 205, p. 459.

Results are given for a sequence of studies of the system ZrO_2–R_2O_3 where R = Yb, Y, Er, Ho, Dy, and Gd, using solar furnace thermal equilibration analysis and high temperature X-ray powder diffraction. Liquidus curves were determined at 5 mol% intervals. D.R.W.

Sc_2O_3–HfO_2

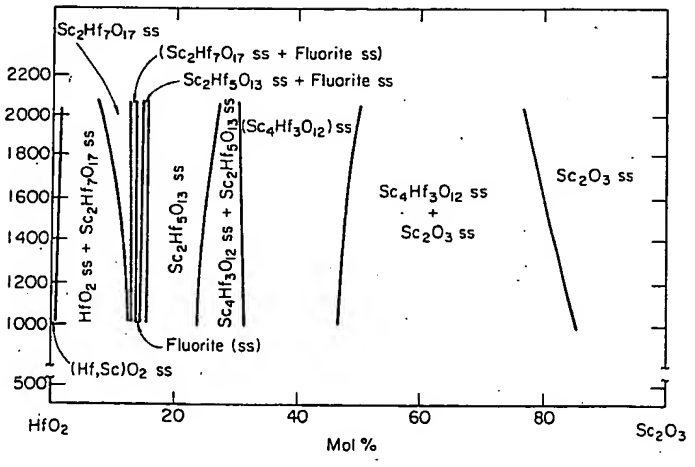

Sm_2O_3–ZrO_2

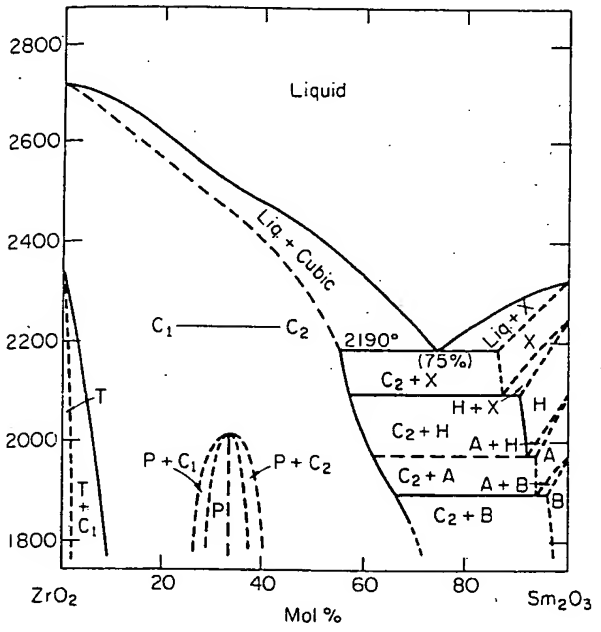

FIG. 5245.–System ZrO_2–Sm_2O_3. A,H = hexagonal ss, X = cubic ss, B = monoclinic ss, C_1, C_2 = cubic ss, P = pyrochlore phase, T = tetragonal ss.

A. Rouanet, *Rev. Int. Hautes Temp. Refract.*, 8 [2] 161 (1971).

The liquidus curve and phase transformations in the solid state were obtained by methods described in Fig. 5232. All dashed curves are estimated. ZrO_2 (99.9, without HfO_2) and Sm_2O_3 (99.9) were the starting materials. For the polymorphism of ZrO_2, see Fig. 4259 and for Sm_2O_3 Ref. 1.

The apparent inflection on the liquidus curve between ZrO_2 and the eutectic is not explained but corresponds roughly to the pyrochlore (P) composition. It may reflect partial ordering in the liquid. The eutectic is at 25%ZrO_2–75%Sm_2O_3, 2190°.

On the rare earth-rich side, the X phase could not be quenched and is difficult to study at high temperature (>2100°) because of the high volatility of Sm_2O_3. Therefore, the homogeneity range of X could not be determined. The X→H transition temperature decreases sharply and the H→A transition is difficult to detect in solid solutions by thermal analysis.

The pyrochlore compound, $Sm_2Zr_2O_7$, disorders above 2000°. The author assumes that the C_1 (cubic fluorite-type) → C_2 (cubic Tl_2O_3-type) transition is continuous with a theoretical boundary at the pyrochlore composition. At the zirconia-rich side, the C_1 phase is completely stabilized with ≈5% Sm_2O_3. The tetragonal (T) → C_1 transition is reversible. The author states that near 6 to 7 mol% Sm_2O_3 an inflection (not explained) appears on the T → C_1 curve.

This diagram differs from Figs. 2387 and 4433, but is more consistent with Figs. 5232 and 5239. Because of polymorphism, the X, H, and A solid solutions of Sm_2O_3 must show eutectoid decomposition giving, respectively, C_2 + H, C_2 + A, and C_2 + B. The diagram is redrawn accordingly.

It appears that additional efforts must be made to obtain a better knowledge of this system especially at high temperature where a diphasic region C_1 + C_2 must exist. Also, a reassessment of the Sm_2O_3-rich side is appropriate. In both cases, long term equilibration at elevated temperature will be necessary.

1. M. Foex and J. P. Traverse, *Rev. Int. Hautes Temp. Refract.*, 3 [4] 429 (1966). J.P.C.

Sm_2O_3–MoO_3

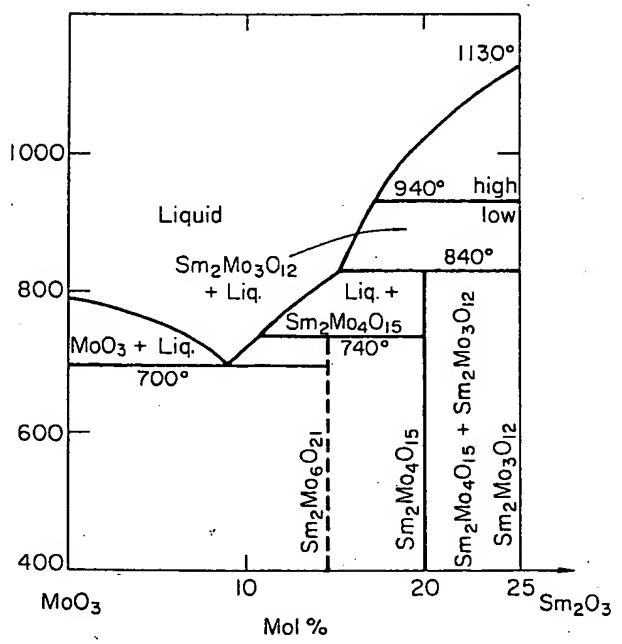

FIG. 5246.–System MoO_3–Sm_2O_3.

S. S. Antonova, I. V. Shakhno, V. E. Plyushchev, *Izv. Vyssh. Uchebn. Zaved., Khim. Khim. Tekhnol.*, 14 [1] 17 (1971).

Samples were prepared by prolonged heating and slow cooling of oxide mixtures in air at 500° to 650°. Analysis was by DTA and X-ray diffractometry. Unit cell parameters of the incongruent melting $Sm_2Mo_4O_{15}$ (1:4) compound are listed. The 1:6 compound, $Sm_2Mo_6O_{21}$, was also identified and a unit cell reported. However, during 120 h heating periods at 720°, 20° below the DTA melting temperature, it was found to completely decompose into MoO_3 and the 1:4 compound. The melting and/or decomposition of this phase is probably time dependent. Polymorphic transition of $Sm_2Mo_3O_{12}$ at 940° was taken into consideration.

This system (at least the 1:6 compound) is qualitatively similar to the systems MoO_3–Y_2O_3 and MoO_3–Er_2O_3 described in the same reference (Figs. 5254 and 5218). D.K.

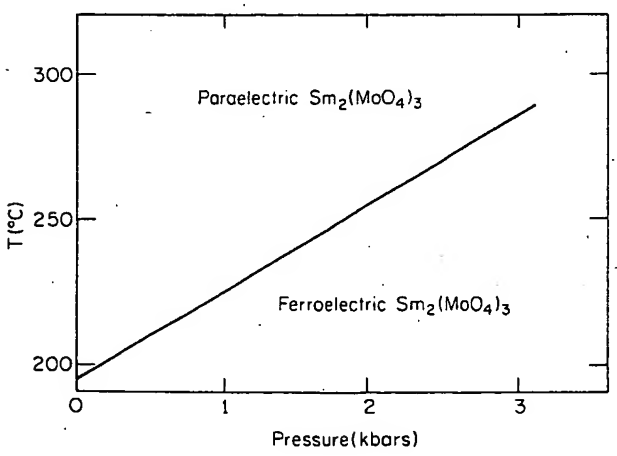

Y_2O_3–ThO_2 (concl.)

FIG. 5250.—System ThO_2–Y_2O_3. H = hexagonal (ss).
F. Sibieude and M. Foex, *J. Nucl. Mater.*, 56 [2] 229 (1975).

The liquidus curves and phase transformations in the solid state were obtained by methods described in Fig. 5231. The diagram is tentative and based on experimental results obtained by thermal analysis and high temperature X-ray diffraction and on data for the polymorphism of Y_2O_3.[1] The liquidus curve is characterized by a eutectic in the Y_2O_3-rich side (≈15%ThO_2–85%Y_2O_3) at ≈2400°.

This diagram resembles the system ThO_2–Er_2O_3 (Fig. 5215) except that the solution of ThO_2 is greater in C-Y_2O_3 and smaller in H-Y_2O_3 than in C-Er_2O_3 and H-Er_2O_3. The limits of Y_2O_3 and ThO_2 dissolution, respectively, in C-ThO_2 and C-Y_2O_3 differ from previous results (Fig. 2389). Beacuse of the use of high temperature X-ray diffraction and thermal analysis, this diagram must be considered as the best available.

1. M. Foex and J. P. Traverse, *Rev. Int. Hautes Temp. Refract.*, 3 [4] 429 (1966). J.P.C.

Y_2O_3–ZrO_2

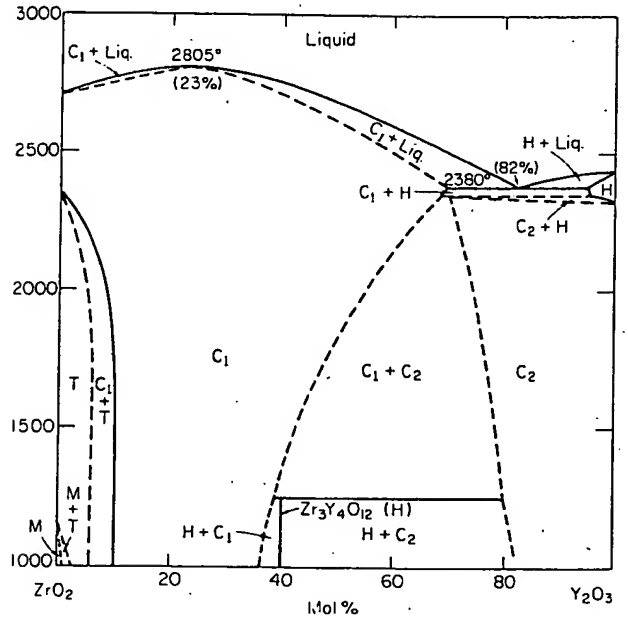

FIG. 5251.—System ZrO_2–Y_2O_3. C_1 = cubic ss of the CaF_2 type, C_2 = cubic ss of the Tl_2O_3 type, H = hexagonal structure, T = tetragonal structure, M = monoclinic structure.
A. Rouanet, *Rev. Int. Hautes Temp. Refract.*, 8 [2] 161 (1971).
S. R. Skaggs, Tech. Rept., SC-RR-72-0031, Jan. 1972, p. 89.

This system has been studied extensively by numerous workers, especially A. Rouanet and S. R. Skaggs, within the very high temperature range. Rouanet obtained liquidus curves and phase transitions by methods described in Fig. 5232. Skaggs melted samples by laser heating. In both studies liquidus temperatures were determined from cooling curves obtained using automatic pyrometers (0.65 μm). Rouanet obtained cooling curves in good blackbody conditions. Melting points (Al_2O_3, 2054°; Y_2O_3, 2440°) provided standards for the pyrometer. Skaggs used published emissivity values (0.84 for ZrO_2 and 0.96 for Y_2O_3). Liquidus temperatures differ in some regions by more than 100°. Earlier diagrams (Figs. 4437(*A*) and (*B*)) show a liquidus maximum reported also by Noguchi.[1] After Rouanet, the composition and temperature of the liquidus maximum are, respectively, 77 mol% ZrO_2-23 mol% Y_2O_3 and 2805°. The solidus curve of Skaggs is inconsistent with the liquidus maximum, illustrating the difficulty of good temperature measurements at extreme temperatures.

Other differences are evident between the two diagrams; (1) at the yttrium oxide-rich side, the cubic (C_2 → hexagonal H) phase transition (T = 2330°)[2] is not shown, (2) Rouanet found a eutectic (2380°, 18 mol% ZrO_2 - 82 mol% Y_2O_3) and Skaggs a peritectic (2483°, same composition), and (3) the major conflict is the existence of a two-phase region between the cubic fluorite-type solid solution (C_1) and the cubic Tl_2O_3-type solid solution (C_2).

In both studies, the pyrochlore compound ($Y_2Zr_2O_7$) postulated in Fig. 2390 was not found. Recently, Ref. 3 has shown that long time annealing (2 weeks, ≈1200°) of $2ZrO_2$:Y_2O_3 mixtures does not yield the ordered pyrochlore compound. However, the hexagonal compound, $Zr_3Y_4O_{12}$, was found, which decomposes above 1250° ±60°.

Using the data of Rouanet and Skaggs, and of Refs. 3 to 5, this tentative diagram was constructed by the compiler (see also Fig. 5252). Additional studies are required to delimit such biphasic regions as C_1 + C_2, C_1 + H, C_2 + H (H, ordered compound, $Zr_3Y_4O_{12}$). Liquidus curves are after Rouanet.

1. T. Noguchi; p. 249 in Advances in High Temperature Chemistry, Vol. 2. Edited by L. Eyring, Academic Press, New York, 1969.
2. M. Foex and J. P. Traverse, *Rev. Int. Hautes Temp. Refract.*, 3 [4] 429 (1966).
3. S. P. Ray and V. S. Stubican, *Mater. Res. Bull.*, 12 [5] 549 (1977).
4. R. Ruh, K. S. Mazdiyasni, and H. O. Bielstein; presented at the 70th Annual Meeting, The American Ceramic Society, Chicago, Ill., May 1968. (Basic Science Div. No. 65–B–68; for abstract see *Am. Ceram. Soc. Bull.*, 47 [4] 366 (1968).
5. O. Sardi, Ph.D. Thesis, University of Indiana (1969). J.P.C.

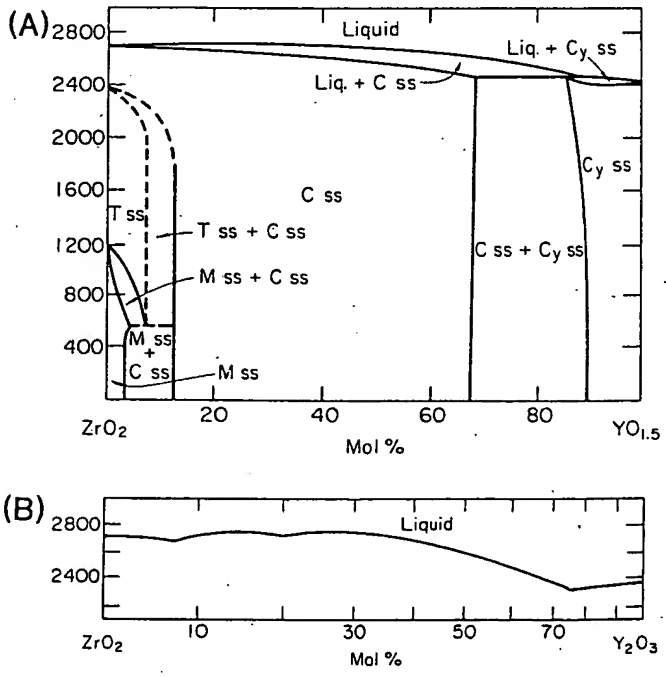

FIG. 5252.—System ZrO_2–$YO_{1.5}$. (*A*) Composite diagram, (*B*) liquidus curve from Ref. 2.
K. K. Srivastava, R. N. Patil, C. B. Choudhary, K. V. G. K. Gokhale, and E. C. Subbarao, *Trans. J. Br. Ceram. Soc.*, 73 [3] 85 (1974).

Twenty compositions across the entire system were prepared at 2000° using an oxyacetylene furnace. Analysis was by subsequent X-ray diffraction at room temperature. Quantitative DTA was used to observe transformations. The experimental results confirm a

YB_2O_3–HfO_2 (concl.)

FIG. 5255.—System HfO_2–Yb_2O_3. C = Tl_2O_3-type structure, F = fluorite-type structure.

E. B. Perova, A. A. Samoilenko, F. M. Spiridonov, L. N. Komissarova, *Zh. Neorg. Khim.*, 17 [10] 2846 (1972); *Russ. J. Inorg. Chem. (Engl. Transl.)*, 17 [10] 1492 (1972).

This system was examined from 1000° to 1800° by X-ray diffraction. Samples were coprecipitated and prepared at 2 to 2.5 mol% intervals across the system. No compounds were observed, all solid solutions are cubic, the C being Tl_2O_3-type, the F being fluorite-type. A linear relation was found between the lattice parameters of the solid solutions and the composition at the various annealing temperatures. The monoclinic↔tetragonal phase transition is not shown for HfO_2 ss. D.R.W.

Yb_2O_3–ThO_2

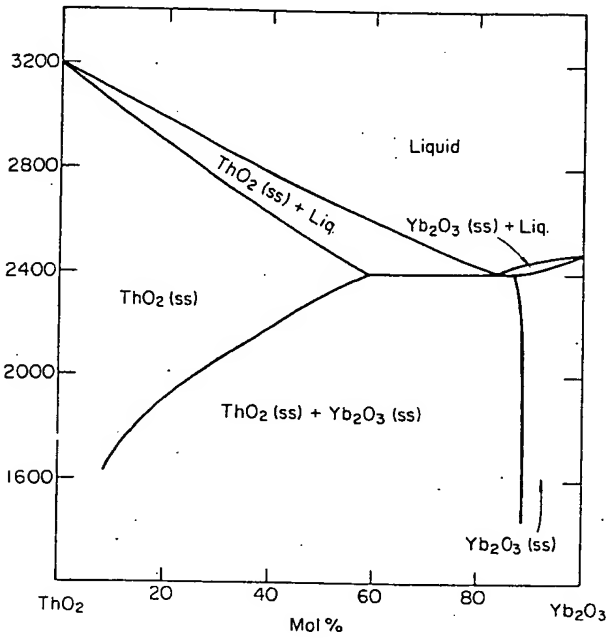

FIG. 5256.—System ThO_2–Yb_2O_3.
F. Sibieude and M. Foex, *J. Nucl. Mater.*, 56 [2] 229 (1975).

The liquidus curve was obtained by methods described in Fig. 5231. This diagram is tentative and based on experimental results obtained by thermal analysis and high temperature X-ray diffraction. The solidus and liquidus curves between ThO_2 and 55%ThO_2-45%Yb_2O_3 are estimated.

The liquidus curve is characterized by a eutectic on the Yb_2O_3-rich side (≈15%ThO_2-85%Yb_2O_3) at 2400°.

The only solid phases are cubic ThO_2 and cubic Yb_2O_3. On the Yb_2O_3-rich side the solubility of C-ThO_2 in C-Yb_2O_3 is independent of the temperature: 10 mol% C-ThO_2 in C-Yb_2O_3 between 1400° and 2200°. On the thoria-rich side the solubility of C-Yb_2O_3 increases from 10% at 1600° to 60% at 2400°. J.P.C.

Yb_2O_3–ZrO_2

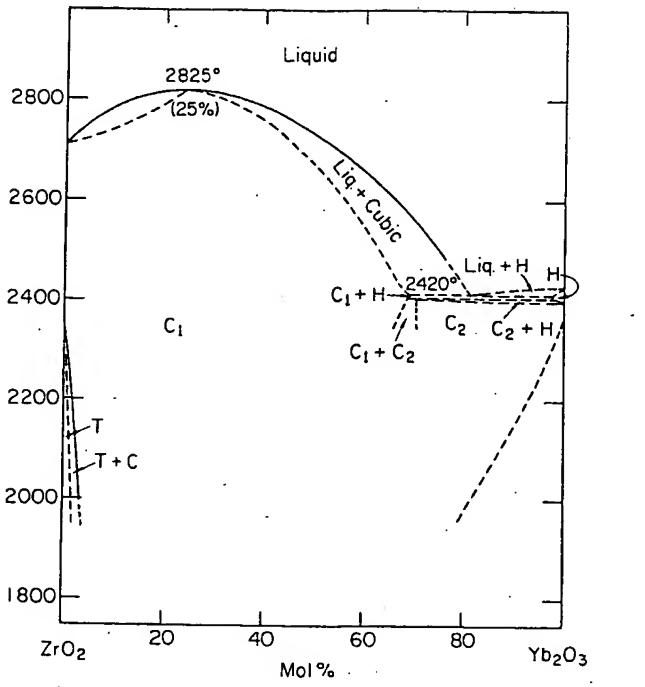

FIG. 5257.–System ZrO_2–Yb_2O_3. H = hexagonal ss, C_1 and C_2 = cubic ss phases, T = tetragonal ss.
A. Rouanet, *Rev. Int. Hautes Temp. Refract.*, 8 [2] 161 (1971).

The liquidus curve was obtained by the thermal analysis device described in Fig. 5232. All dashed curves are estimated. ZrO_2 (99.9% without HfO_2) and Yb_2O_3 (99.9%) were the starting materials. On the zirconia-rich side, the tetragonal (T) → C_1 transition is reversible.

At high temperature (>1800°), solid solutions vary from a cubic fluorite structure (C_1) to a cubic Tl_2O_3-type structure (C_2). The author states that the theoretical boundary is at the ZrO_2:Yb_2O_3 composition but this is questionable. A biphasic region, C_1 + C_2, must exist but it may be difficult to determine (e.g. sluggish solid state reactions). The dashed line at the Yb_2O_3-rich side reflects a thermal effect attributed by the author to the dissociation of Yb_2O_3. The ordered compound $Zr_3Yb_4O_{12}$[1] was not observed, perhaps due to the low temperature limit of this study (≈1800°).

By carefully studying cooling curves of Yb_2O_3, Traverse[2] suggested that a C→H phase transition could exist just below the melting point. This diagram represents a tentative revision of Fig. 4440.

1. M. R. Thornber and D. J. M. Bevan, *J. Solid State Chem.*, 1 [3-4] 536 (1970).
2. J. P. Traverse, Thesis, CNRS, AO5879, June 1971. J.P.C.

$MgO–CeO_2–ZrO_2$ (concl.)

FIG. 5418.—System CeO_2–MgO–ZrO_2. (*A*) 1700° section, (*B*) 1500° section, (*C*) 1300° section, (*D*) 1200° section.
V. Longo and L. Podda, *Ceramurgia*, 1 [2] 92 (1971).

At least 227 compositions were formulated from CeO_2 (99.9%), $MgCO_3$ (99.8%), and ZrO_2 (99.7%, excluding ≈2% HfO_2). These were pressed into disks and fired in air according to the following schedules:

(*a*) 1400°, 250 h, then 8 h at 1600° and 1700°
(*b*) 1400°, 500 h, then 150 h at 1500°
(*c*) 1400°, 750 h, then 1000 h at 1400° and 1200 h at 1300°
(*d*) 1400°, 1000 h, then 1200°, 1500 h, and 1100°, 1500 h

Temperature was measured by calibrated Pt–Pt10Rh thermocouples. More than 1000 samples (quenched in air) were analyzed by reflected light microscopy and powder X-ray diffraction and sections for the 1700°, 1600°, 1500°, 1400°, 1300°, 1200°, and 1100° isotherms were constructed accordingly. Only four of these sections deemed sufficiently different are included here.

CeO_2 accepts little MgO in solid solution. The extent of a tetragonal ZrO_2 solid solution with MgO is considered minimal in general accord with Fig. 4339 but not with Figs. 271 and 2317. With decreasing temperature, the ternary cubic solid solution field progressively decreases in extent until equilibria are dominated by the binary phase assemblages.

These isothermal sections were constructed, apparently assuming that cerium remains 4+ (i.e. CeO_2) within binary and ternary solid solutions. Reduction of some of the cerium to 3+ is probable at the elevated temperatures, and, hence, these sections must be considered as isobaric-isothermal equilibria in the system CeO_2–Ce_2O_3–MgO–ZrO_2 projected onto the CeO_2-MgO-ZrO_2 plane. T.N.

$MgO–SiO_2–V_2O_5$

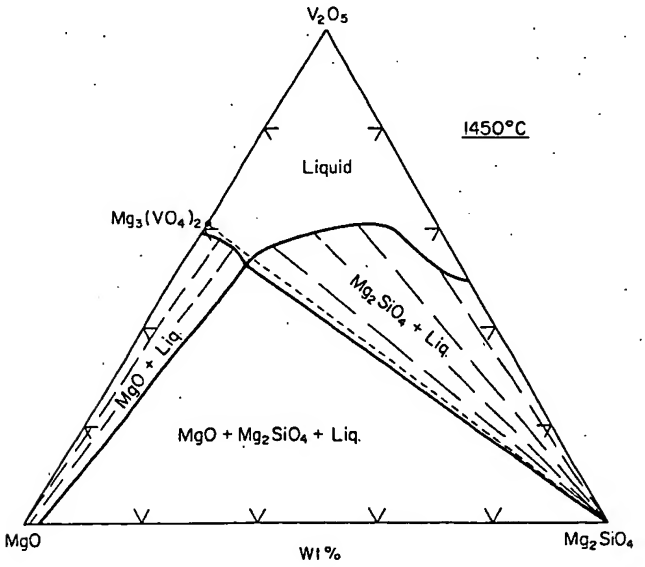

FIG. 5419.—System MgO–Mg_2SiO_4–V_2O_5 1450° section.
M. Carter and N. H. Brett, *Trans. J. Br. Ceram. Soc.*, 72 [5] 203 (1973).

More than fifty compositions were reacted in the solid state and when liquid was present they were quenched. Experimental methods are described in the commentary for Fig. 5486. This isothermal section illustrates the effect of V_2O_5 on refractories based on MgO and Mg_2SiO_4 (forsterite). The location of the 1450° isotherm and its intersection with the MgO-Mg_2SiO_4-liquid boundary curve yields a ternary point given at 39% MgO, 11% M_2S, and 50 wt% V_2O_5. See Figs. 5485 and 5486 for additional aspects of this work. T.N.

$MnO–SiO_2–ZrO_2$

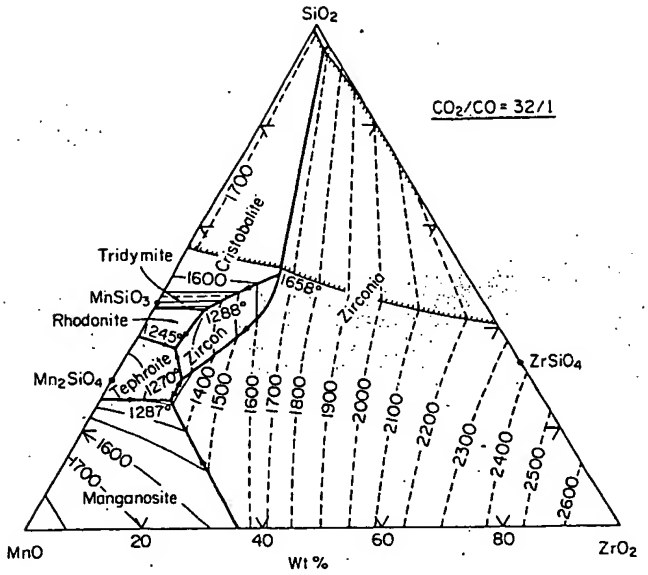

FIG. 5420.—System MnO–ZrO_2–SiO_2.
R. L. Shultz and A. Muan, *J. Am. Ceram. Soc.*, 54 [10] 504 (1971).

Phase relations in the liquidus region of the system MnO–ZrO_2–SiO_2 were determined by the quenching technique. Starting mixtures were prepared from high-purity chemicals heated at 1400° (air, 12 h) within Mn-saturated Pt crucibles. The glassy products were then homogenized and treated at 1200° (air, 48 h) and at 1150° (a reducing atmosphere, 48 h). Pressed pellets wrapped with fine Pt wire were equilibrated at sufficiently low oxygen pressures (CO_2-CO atmospheres of controlled CO_2/CO ratios) to keep most of the Mn in the divalent state. Calibrated Pt–PtRh thermocouples were used to measure temperature with an estimated accuracy of ±5°. Phase assemblages of the quenched samples were determined by microscopic and X-ray examination.

The diagram shows the liquidus surface of the system in a CO_2-CO atmosphere of CO_2/CO ratio = 32/1. Heavy lines are boundary curves between adjacent primary phase areas, as labelled on the diagram; light lines are liquidus isotherms, and lines with shading on one side are outlines of a two-liquid region. The system is not strictly ternary as the oxidation state of Mn is variable. Nevertheless, "invariant" points are generated by the intersections of univariant boundary curves and the oxygen isobaric section. These ternary invariant points are summarized below.

Temp. (°C)	Phases + liquid	Liquid composition (wt%) MnO	ZrO_2	SiO_2
1287	Mn_2SiO_4, MnO, ZrO_2	62	12	26
1270	Mn_2SiO_4, ZrO_2, $ZrSiO_4$	58	12	30
1245	Mn_2SiO_4, $ZrSiO_4$, $MnSiO_3$	56	8	36
1288	$ZrSiO_4$, $MnSiO_3$, SiO_2	47	9	44
1658	$ZrSiO_4$, ZrO_2, SiO_2	31	19	50
1670	$ZrSiO_4$, SiO_2, two liquids	30 1	19 4	51 95

A.M.

$ZnO–SiO_2–Nb_2O_5$ (concl.)

FIG. 5436.—System $ZnO–SiO_2–Nb_2O_5$. Z = ZnO, N = Nb_2O_5, S = SiO_2, ZN = $ZnNb_2O_6$, Z_3N = $Zn_3Nb_2O_8$, Z_2S = Zn_2SiO_4, Z_2N_{17} = $Zn_2Nb_{34}O_{87}$. Ternary liquidus diagram (*A*) and binary systems Z_3N - Z_2S (*B*), ZN - Z_2S (*C*), and ZN - S (*D*). (*E*) and (*F*) show subsolidus tie lines at 1000° to 1085° and 1085° to 1200°, respectively.
R. R. Dayal, *J. Less-Common Met.*, 29 [1] 1 (1972).

The ternary system $ZnO–Nb_2O_5–SiO_2$ was studied using hot-stage microscopy (liquidus region) and quenching (subsolidus region) techniques. Oxide mixtures were prepared for study by grinding under acetone and firing at 1000° for 18 h with successive homogenization. Liquidus temperatures were reported to be accurate to ±5°. Subsolidus charges were held for an unspecified duration in a platinum tube furnace and quenched in air for later X-ray diffraction identification. Pertinent details concerning the liquidus phase relations are given in the table:

Composition (wt%)*				
ZnO	Nb_2O_5	SiO_2	Temp. (°C)	Phases present
53.0	43.8	3.2	1248	Z + Z_3N + α-Z_2S + liquid
48.0	46.5	5.5	1244	Z_3N + α-ZN + Z_2S + liquid
44.0	41.5	14.5	1264	Z_2S + α-ZN + S + liquid
17.0	79.0	4.0	1352	β-ZN + Z_2N_{17} + S + liquid
9.8	88.0	2.2	1407	Z_2N_{17} + N + S + liquid

*All compositions listed were eutectic type.

C.E.S.

$Al_2O_3–CeO_2–ZrO_2$

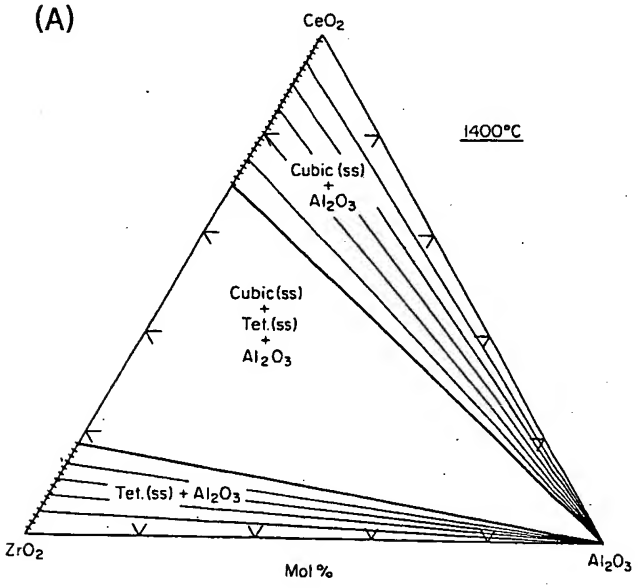

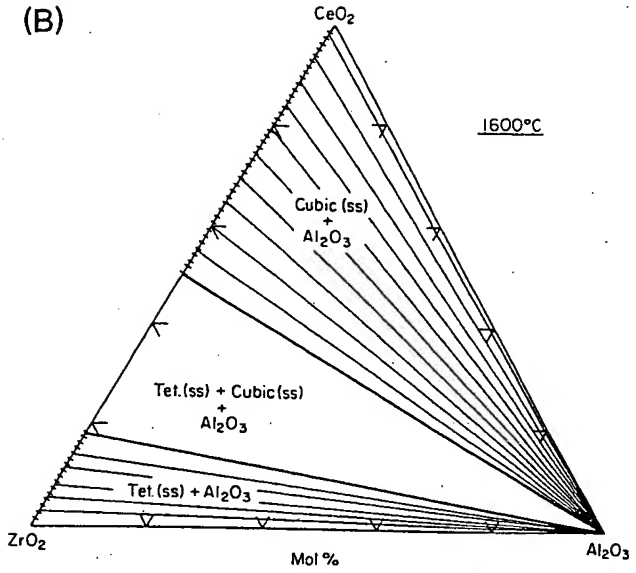

FIG. 5437.—System $ZrO_2–Al_2O_3–CeO_2$. (*A*) Subsolidus isothermal sections at 1400°. (*B*) Subsolidus isothermal sections at 1600°.
V. Longo and L. Podda, *Ceramurgia*, 1 [1] 11 (1971).

More than 200 specimens were formulated from ZrO_2, CeO_2, and Al_2O_3, all having a stated purity of >99.8% excluding ≈2% HfO_2 in the former. These were mixed, pressed into disks, and fired in air at 1400° (1000 h) and at 1500° (250 h) followed by 1600° (8 h). Specimens were quenched in air and analyzed by reflected light microscopy and X-ray powder diffraction.

Diagrams (*A*) and (*B*) show subsolidus isothermal sections at 1400° and 1600°, respectively. Mutual solid solubility between Al_2O_3 and ZrO_2 could not be detected at the 1 mol% level in agreement with Figs. 4377 and 4378. ZrO_2-Al_2O_3 specimens did not melt up to 1730°, suggesting a solidus temperature higher than that given in Fig. 4377. Solid solution in the system $CeO_2–Al_2O_3$ also was not detected. However above 1600° in air (and at lower temperatures at lower P_{O_2}) the compounds $Ce^{3+}AlO_3$ and $Ce_2O_3 \cdot 11Al_2O_3$ are reported to be stable.

These isothermal sections were constructed, apparently assuming that CeO_2 and "CeO_2"/ZrO_2 solid solutions are stoichiometric. CeO_2, however, undergoes slight reduction at high temperatures even in air (e.g. Ref. 1). "CeO_2"/ZrO_2 solid solutions undergo more substantial reduction in air (e.g. Ref. 2). Thus, these sections must be considered as isobaric-isothermal equilibria in the system $CeO_2–Ce_2O_3–Al_2O_3–ZrO_2$ projected onto the $CeO_2–Al_2O_3–ZrO_2$ plane.

1. R. J. Panlener and R. N. Blumenthal, AEC Report 000-1441-18 (1972).
2. T. Negas, R. S. Roth, C. L. McDaniel, H. S. Parker, and C. D. Olson, *Proc. Rare Earth Res. Conf., 12th*, 2, 605 (1976). Edited by C. E. Lundin.

T.N.